1624 *Biochemistry* **2011,** *50,* 1624–1633
DOI: 10.1021/bi101913m

BIOCHEMISTRY
including biophysical chemistry & molecular biology
Article

Ubiquitin in Motion: Structural Studies of the Ubiquitin-Conjugating Enzyme∼Ubiquitin Conjugate†

Jonathan N. Pruneda,[‡,∥] Kate E. Stoll,[‡,∥,§] Laura J. Bolton,[‡] Peter S. Brzovic,[‡] and Rachel E. Klevit*[,‡,§]

[‡]*Department of Biochemistry and* [§]*Biomolecular Structure and Design Program, University of Washington, Seattle, Washington 98195, United States.* [∥]*These authors contributed equally to this work.*

Received November 30, 2010; Revised Manuscript Received January 10, 2011

ABSTRACT: Ubiquitination of proteins provides a powerful and versatile post-translational signal in the eukaryotic cell. The formation of a thioester bond between ubiquitin (Ub) and the active site of a ubiquitin-conjugating enzyme (E2) is critical for the transfer of Ub to substrates. Assembly of a functional ubiquitin ligase (E3) complex poised for Ub transfer involves recognition and binding of an E2∼Ub conjugate. Therefore, full characterization of the structure and dynamics of E2∼Ub conjugates is required for further mechanistic understanding of Ub transfer reactions. Here we present characterization of the dynamic behavior of E2∼Ub conjugates of two human enzymes, UbcH5c∼Ub and Ubc13∼Ub, in solution as determined by nuclear magnetic resonance and small-angle X-ray scattering. Within each conjugate, Ub retains great flexibility with respect to the E2, indicative of highly dynamic species that adopt manifold orientations. The population distribution of Ub conformations is dictated by the identity of the E2: the UbcH5c∼Ub conjugate populates an array of extended conformations, and the population of Ubc13∼Ub conjugates favors a closed conformation in which the hydrophobic surface of Ub faces helix 2 of Ubc13. We propose that the varied conformations adopted by Ub represent available binding modes of the E2∼Ub species and thus provide insight into the diverse E2∼Ub protein interactome, particularly with regard to interaction with Ub ligases.

Covalent attachment of the 8.6 kDa ubiquitin (Ub)[1] to target proteins is an essential step in eukaryotic signaling pathways. The type of Ub modification can vary, inducing distinct signals. For example, monoubiquitination may elicit a signal for protein transport, while polyubiquitination (attachment of a chain of Ubs to the target) may mark a protein for proteasome-mediated degradation. Covalent attachment of Ub to a substrate proceeds through a multienzyme process consisting of a Ub-activating enzyme (E1), a Ub-conjugating enzyme (E2), and a Ub ligase (E3) (*1*). The human genome contains two Ub E1s, ∼35 E2s, and many hundreds of E3s (*2*). Despite the large number of E2s, they share significant similarity at the level of both sequence and structure. E2s play a central role in the ubiquitination cascade, shuttling Ub from an E1 to an E3−substrate complex. The E2 holds Ub in its activated form via formation of a thioester bond between the carboxy terminus of Ub and the E2's active site cysteine (denoted as E2∼Ub).

The small size and high solubility of many E2s have made them prime candidates for structural investigations. There are ∼100 structures of E2s in the Protein Data Bank (PDB), and 23 of the ∼35 human E2s have had their structures deposited. This wealth of information reveals that all E2s are related by their conserved catalytic cores that fold into an α/β topology. Significantly fewer structures of E2∼Ub complexes have been determined, probably because of the technical challenges that the labile thioester conjugate poses. There are at present five structures of E2∼Ub conjugates or close structural analogues that have been determined by X-ray crystallography or NMR: Ubc13∼Ub [PDB entry 2GMI (*3*)], Ubc1∼Ub [PDB entry 1FXT (*4*)], UbcH8∼Ub [PDB entry 2KJH (*5*)], and UbcH5b∼Ub [PDB entries 3A33 (*6*) and 3JW0 (*7*)]. In each case, the backbones of the E2 and Ub moieties are not significantly altered from their free structures. However, each structure presents a unique relative orientation of the E2 and Ub units.

Despite the wealth of atomic-level structural information about E2s, E2−E3 complexes, and a growing number of E2∼Ub conjugates, the ways in which E3s catalyze the transfer of Ub from an E2∼Ub conjugate remain poorly understood. It is clear that one function of the E3 is to bind a substrate simultaneously with binding an E2∼Ub conjugate, thereby bringing the two components into proximity. However, even in the absence of a protein substrate, E3s have been shown to enhance the rate at which Ub is released from an E2∼Ub conjugate, presumably via reaction of the thioester bond with solvent or buffer components (*8*, *9*). Although this so-called hydrolysis or release rate may not be the mechanistic equivalent of the reaction involving a substrate lysine side chain, the ability of an E3 to enhance the reactivity of an E2∼Ub conjugate suggests that an

†This work was supported by National Institutes of Health Grant R01 GM088055 (R.E.K.), U.S. Public Health Service (PHS) Grant NRSA T32 GM008268 (K.E.S. and J.N.P.), and PHS Grant NRSA 2T32 GM007270 from the National Institute of General Medical Sciences (J. N.P.).

*To whom correspondence should be addressed: University of Washington, Box 357350, Seattle, WA 98195. Telephone: (206) 543-5891. Fax: (206) 543-8394. E-mail: klevit@uw.edu.

[1]Abbreviations: Ub, ubiquitin; E2, ubiquitin-conjugating enzyme; E3, ubiquitin ligase; E1, ubiquitin-activating enzyme; RING, Really Interesting New Gene; HECT, homologous to the E6AP carboxy terminus; NMR, nuclear magnetic resonance; SAXS, small-angle X-ray scattering; PRE, paramagnetic relaxation enhancement.

 Published on Web 01/12/2011

E2 active site can somehow be tuned in response to E3 binding. As a step toward understanding how an E3 ligase regulates E2∼Ub conjugate activity, a more complete description of the E2∼Ub conjugate is needed. Furthermore, under steady state equilibrium the conjugated form of E2s are likely to be the predominant form in vivo because E1 is efficient at maintaining E2s in the conjugated state, as exemplified by human Ubc2b (*10*, *11*). Thus, E3s and other cellular proteins are more likely to encounter E2∼Ub conjugates than free E2s. We have chosen to focus on UbcH5c and Ubc13, two highly related E2 enzymes (45.6% identical and 61% similar sequences) with divergent activities and specificities (Figure S3 of the Supporting Information). Orthologues of both UbcH5c and Ubc13 play key roles in all organisms from yeast to humans (*12*). These two E2s are well-characterized, with structures determined for each in their free and Ub-conjugated states [Ubc13, PDB entries 1J7D (*13*) and 2GMI; UbcH5, PDB entries 1X23 and 3A33], both alone and in complex with interacting proteins. These studies and our own make use of an active site Cys-to-Ser mutation to generate a more stable oxyester-linked E2-O∼Ub conjugate. In this study, we use NMR chemical shift mapping, site-specific paramagnetic labeling, and small-angle X-ray scattering (SAXS) to examine the ensemble of E2∼Ub conformations populated by UbcH5c∼Ub and Ubc13∼Ub conjugates in solution. Characterization of the E2∼Ub conjugate in solution will facilitate future structural studies with interacting proteins, including E3 ligases.

EXPERIMENTAL PROCEDURES

Plasmids, Protein Expression, and Purification. N-Terminally His_6-tagged Ubc13 was expressed from the pET24 vector. UbcH5c was expressed from the pET28N vector. UbcH5c and BRCA1_1−112/BARD1_25−139 were purified as previously described (*14*). Proteins were expressed in *Escherichia coli* (BL21 star DE3 cells) at 37 °C and induced with 1 mM IPTG for 4 h or at 16 °C induced with 200 μM IPTG for 18 h. His_6-Ubc13 was purified using a Ni^{2+} affinity column, followed by size exclusion chromatography on SDX75 resin in 25 mM sodium phosphate, 150 mM NaCl buffer (pH 7.0), the buffer used for all NMR experiments.

Spin-Label Modification. Four mutant forms of Ub were generated using site-directed mutagenesis (K11C, D39C, K48C, and K63C) to incorporate a cysteine for chemical modification with the thiol-reactive relaxation probe 4-(2-iodoacetamido)-TEMPO (Sigma-Aldrich) to form a covalently linked, nontransferable adduct. Reactions between TEMPO and each cysteine mutant of Ub were performed at 25 °C overnight at a 1:5 Ub:TEMPO molar ratio. Reaction yields were quantified by MALDI-MS; in all cases, the reaction went essentially to completion (>95%). Unreacted TEMPO was removed by dialysis prior to the conjugation reaction. We confirmed paramagnetic activity by incorporating a spin-label into [^{15}N]Ub K63C and recording HSQC spectra before and after reducing the nitroxide probe with ascorbate. Comparison of the [^{15}N]Ub K63SL ascorbate-reduced spectrum with that of wild-type Ub showed little spectral perturbation associated with the cysteine mutation and subsequent modification with the spin-label.

Formation of the E2∼Ub Conjugate. To characterize the conjugated forms of E2s UbcH5c and Ubc13, we used an active site Cys-to-Ser mutation (C85S in UbcH5 and C87S in Ubc13) to generate an oxyester between the C-terminus of Ub and the E2. The resulting bond is only one atom different from the wild-type thioester and significantly more stable. All structural work described in this study utilized the active site Cys-to-Ser mutation; the conjugates formed with these E2s are denoted as E2-O∼Ub conjugates. NMR studies of the UbcH5c-O∼Ub conjugate were performed in the context of the S22R mutation to prevent noncovalent Ub binding (*15*). [^{15}N]E2-O∼Ub oxyester conjugates were generated by reaction of 5−10 μM E1, 600 μM TEMPO-modified or wild-type Ub, 300 μM [^{15}N]E2s ([^{15}N]C85S/S22R-UbcH5c or [^{15}N]C87S-Ubc13), 5 mM $MgCl_2$, and 2.5 mM ATP at 30 °C for 3−6 h. E2-O∼Ub conjugates were purified from unreacted material by gel filtration on SDX75 resin, and the homogeneity of the E2-O∼Ub species was confirmed by sodium dodecyl sulfate−polyacrylamide gel electrophoresis. Two-dimensional (2D) ^{1}H−^{15}N TROSY-HSQC spectra were recorded for samples containing 150 μM E2∼Ub conjugate before and after reduction of the paramagnetic probe with 5 molar equiv of ascorbate.

NMR Spectroscopy. Chemical shift perturbation and paramagnetic relaxation enhancement (PRE) data were collected at 25 °C on a Bruker 500 MHz AVANCE II NMR spectrometer (University of Washington). Relaxation data were collected at 25 °C on a Varian 600 MHz INOVA NMR spectrometer (Pacific Northwest National Laboratories, Richland, WA). Data processing and analysis were performed using NMRPipe (*16*) and NMRView (*17*). Peak intensities were measured in NMRView, and intensity ratios for individual NH peaks in the active and ascorbate-reduced spectra (I/I_{red}) were calculated. Spin-label-affected E2 resonances were identified as those with a peak intensity ratio of < 0.70. In general, this cutoff was approximately one standard deviation from the mean. Chemical shift perturbations observed by 2D TROSY-HSQC NMR were quantified in parts per million with the equation $\Delta\delta_j = [(\Delta\delta_j^{15}\mathrm{N}/5)^2 + (\Delta\delta_j^{1}\mathrm{H})^2]^{1/2}$.

Small-Angle X-ray Scattering. SAXS data were collected at Stanford Synchrotron Radiation Lightsource beamline 4-2. Data were collected for UbcH5c, the UbcH5c∼Ub conjugate, and the His_6-Ubc13∼Ub conjugate at concentrations of 10, 5, and 0.5 mg/mL in 25 mM sodium phosphate, 150 mM NaCl, and 2 mM DTT (free radical scavenger) (pH 7.0) at 25 °C. Data for His_6-Ubc13 were collected at 7, 5, and 0.5 mg/mL in the same buffer without DTT. Initial data subtraction and averaging were performed with SSRL in-house software and confirmed using PRIMUS (*18*). R_g values calculated from the Guinier plot, the Porod plot, and the $P(r)$ function were all consistent. The $P(r)$ functions were calculated using GNOM (*19*), and theoretical scattering profiles of published structures were calculated using CRYSOL (*20*) and OLIGOMER (*18*). Existing E2∼Ub structures were substituted with the appropriate E2 structure prior to calculation of the theoretical scattering profile. Flexibility analysis using the ensemble optimization method (EOM) (*21*) was performed using RanCh to create a pool of 10000 random E2∼Ub conformations based upon flexibility in Ub residues 72−76. The GAJOE genetic algorithm was used as described previously to select an ensemble of 20 conformations that, together, best fit the scattering data (*21*). SAXS data for free His_6-Ubc13 were used to model a single conformation of the His_6 tag that is consistent with the measured SAXS curve. The His tag model was then used to represent the Ubc13 component within the His-Ubc13∼Ub RanCh/GAJOE analysis.

RESULTS

We have previously reported the NMR chemical shift perturbations observed for the UbcH5c-O∼Ub conjugate relative to the free protein counterparts (*15*). The most notable features of the UbcH5-O∼Ub conjugate were its asymmetric perturbations in which significant chemical shift perturbations were observed to emanate away from the active site in the E2 but were highly localized to the extreme C-terminus of the Ub moiety. Ub chemical shifts beyond the C-terminal residues are small (< 0.05 ppm). While more than one-third (45 of 126) of UbcH5c resonances are shifted by more than one peak width, only 12 are shifted by greater than one standard deviation from the mean. Mapping these 12 residues onto the three-dimensional (3D) structure reveals a spotted surface spanning the crossover helix (helix 2), the active site, loop 5 (residues 75−77), and the C-terminal helices (helices 3 and 4) (see Figure 3C of ref *15*). Such a distributed perturbation surface is consistent with either a conformational adjustment in interior hydrophobics (aromatics) or a dynamic UbcH5c-O∼Ub species in which activated Ub makes transient contact with multiple E2 surfaces.

Mapping the Ubc13∼Ub Conjugate Interface by Chemical Shift Perturbation Analysis. To allow for study of the Ubc13-O∼Ub conjugate by NMR, the 2D HSQC-TROSY spectrum of the [^{15}N]Ubc13-O∼Ub conjugate was assigned. The lifetime of the Ubc13-O∼Ub species in solution is too short for collection of 3D spectra such as HNCA or HNCACB. On the basis of the observation that E2 structures do not change significantly in their Ub-conjugated states (*3*, *5*, *6*), we turned to HNCO spectra that can be recorded with shorter acquisition times. The chemical shifts of backbone carbonyl groups are largely determined by the structure in which they are found, so the spectrum of conjugated Ubc13 could be assigned by matching HNCO carbonyl assignments between free and conjugated Ubc13 (Table S1 of the Supporting Information). Comparison of the ^{1}H and ^{15}N chemical shifts of the free and conjugated protein reveals significant chemical shift perturbations (CSPs) in backbone amide resonances beyond the active site of Ubc13 (Figure 1A,C). In contrast to the UbcH5-O∼Ub conjugate, [^{15}N]Ub exhibits significant CSPs beyond its C-terminal tail when conjugated to Ubc13 (Figure 1B−D).

When mapped onto the crystal structure of the Ubc13-O∼Ub conjugate (PDB entry 2GMI), the CSPs resulting from the conjugation of Ub to Ubc13 reveal discrete surfaces on each protein component. The surface on Ubc13 is comprised of helix 2 ("crossover helix", residues 100−114), loop 8 (residues 114−123), and, to a lesser extent, the penultimate C-terminal helix (see Table S2 of the Supporting Information for residue-level information). The I44 hydrophobic surface of Ub is perturbed upon conjugation to Ubc13 (Figure 1C,D and Table S2 of the Supporting Information). The chemical shifts in Ub arising from conjugation to Ubc13 are remarkably different from those observed for conjugation to UbcH5c, in both profile and magnitude (Figure 1D). The perturbations observed when Ubc13 is conjugated to Ub are not congruent with those expected for an E2∼Ub complex in an extended state, as observed in the crystal structure of the Ubc13-O∼Ub conjugate. The simplest interpretation of the observed perturbations is that they identify surfaces on Ubc13 and Ub that are in the proximity of each other in the conjugate, suggesting a closed conformation in which the Ub is folded up toward the crossover helix of Ubc13. A similar closed state has been proposed for the yeast Ubc1∼Ub conjugate based on NMR observations (*4*); however, because this E2∼Ub conjugate was created using a wild-type thioester linkage, it suffered from a short half-life and incomplete NMR assignments. The chemical shift perturbations observed for the oxyester forms of the UbcH5-O∼Ub and Ubc13-O∼Ub conjugates allow direct comparison and suggest that the Ubc13-O∼Ub conjugate populates closed conformations more frequently than the UbcH5c-O∼Ub conjugate does.

Mapping the RING E3 Binding Surface of Ubc13 by Chemical Shift Perturbation Analysis. To determine an E3's ability to bind the closed Ubc13-O∼Ub conformation, we measured CSPs for free Ubc13 and the Ubc13-O∼Ub conjugate upon the addition of 1.1 equiv of the minimal RING domains of the heterodimeric RING E3 BRCA1/BARD1. The chemical shift perturbations on [^{15}N]Ubc13 induced by BRCA1/BARD1 binding map to the conventional E3 binding surface comprised of helix 1 and loops 4 and 7 of Ubc13 (Figure 2B and Table S2 of the Supporting Information for residue-level information). Resonances perturbed upon addition of BRCA1/BARD1 to the Ubc13-O∼Ub conjugate map to the same surface as those of free Ubc13. Conjugation-induced CSPs in Ubc13 residues (e.g., D44 and T51) are not affected by E3 binding (Figure 2A). These observations indicate that E3 binding does not preclude or detectably perturb the closed conformation of the Ubc13-O∼Ub conjugate.

E2∼Ub Species Are Highly Dynamic. To observe the resonances of the E2 and Ub moieties simultaneously, UbcH5c-O∼Ub and Ubc13-O∼Ub conjugates were generated using ^{15}N-labeled E2 and ^{15}N-labeled Ub. The ^{1}H−^{15}N HSQC-TROSY spectra of the resulting species display two classes of resonances distinguished by sharper peaks with higher intensities or broader peaks with lower intensities. NMR line widths are a function of T_2 relaxation and therefore reflect the dynamics of individual groups within a protein. An E2∼Ub conjugate in which both proteins behave as a globular complex would be expected to display similar line widths throughout the spectrum. In both UbcH5c-O∼Ub and Ubc13-O∼Ub conjugates, the sharper, more intense resonances arise from the 8.6 kDa Ub subunit (Figure 3A), consistent with Ub behaving as a flexibly tethered protein that is largely independent of the 17 kDa E2 to which it is conjugated.

T_1 and T_2 relaxation times were measured for UbcH5c, Ub, and the UbcH5c-O∼Ub conjugate (Figure 3B). Within the conjugate, T_1/T_2 ratios differed significantly between the UbcH5c and Ub moieties (average values of 26.3 and 14.7, respectively). Average T_1/T_2 values for free UbcH5c and Ub were measured to be 9.2 and 3.3, respectively. The lifetime of the Ubc13-O∼Ub oxyester conjugate (half-life at pH 7 and 25 °C of ∼10 h) did not allow for collection of high-quality ^{15}N T_1 and T_2 relaxation measurements. In summary, both observed line widths and ^{15}N relaxation parameters indicate that the Ub moieties within the UbcH5-O∼Ub and Ubc13-O∼Ub conjugates behave as highly flexible entities in a manner independent of the E2s to which they are attached.

Use of Spin-Labeled Ub in the Investigation of the Solution Conformations of the E2∼Ub Conjugate. While the asymmetric CSPs observed for the UbcH5c-O∼Ub conjugate seem consistent with the dynamic behavior evidenced by the line widths, the implied closed conformations for the Ubc13-O∼Ub conjugate based on CSPs seem to contradict its dynamic behavior. The dynamics indicate that while the Ubc13∼Ub conjugate may populate a closed conformation that gives rise

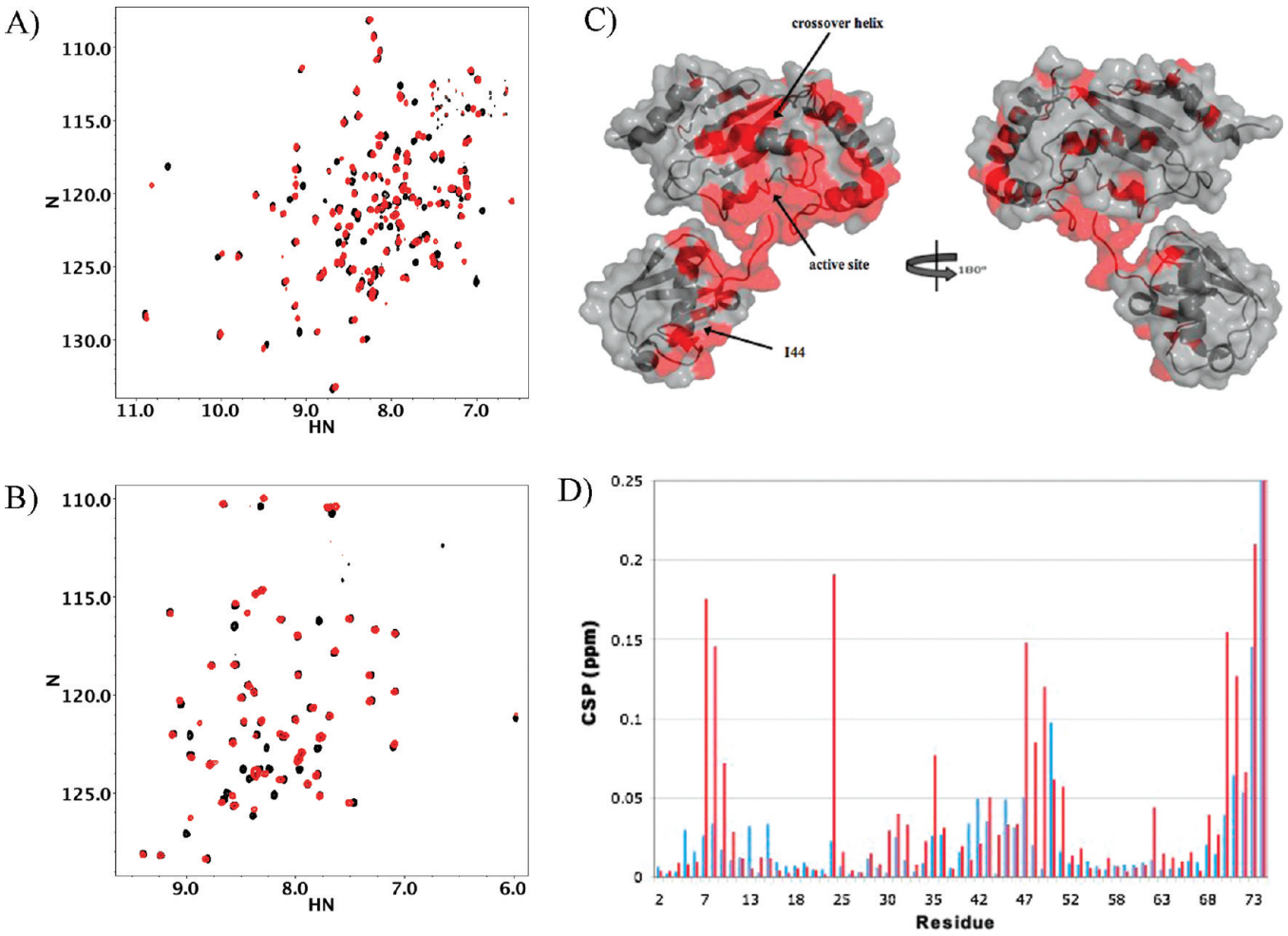

FIGURE 1: Spectral perturbations observed in Ubc13 and Ub upon formation of the Ubc13-O∼Ub conjugate. (A) 2D HSQC-TROSY spectrum of [^{15}N]Ubc13 (black) overlaid with the spectrum of the oxyester-linked [^{15}N]Ubc13-O∼Ub conjugate (red). (B) 2D HSQC-TROSY spectrum of [^{15}N]Ub (black) overlaid with that of the [^{15}N]Ub∼O-Ubc13 conjugate (red). (C) Combined ^{1}H and ^{15}N chemical shift perturbations greater than 0.05 ppm mapped in red on the structure of the Ubc13-O∼Ub conjugate [PDB entry 2GMI with the human Ubc13 structure overlaid (PDB entry 1J7D)]. Perturbations reveal surfaces on both Ubc13 and Ub, suggestive of a protein−protein interaction in which the hydrophobic I44 surface of Ub rotates to meet the surface mapped on Ubc13. (D) Histogram showing Ub CSPs upon activation to Ubc13 (red) and UbcH5c (blue). Comparison of the two profiles reveals differences in both the identity of affected residues and the degree to which they are perturbed.

to the observed CSPs, this conformation must be in equilibrium with others, on a time scale that is consistent with the sharper line widths for Ub. We exploited the lack of cysteines in wild-type Ub to make site-specific cysteine mutations for incorporation of a thiol-reactive paramagnetic nitroxide probe at positions 11 (K11SL), 39 (D39SL), 48 (K48SL), and 63 (K63SL). A spin-label accelerates the T_2 relaxation rate of nearby nuclei, resulting in broadening of line widths in an HSQC-type NMR spectrum, termed the paramagnetic relaxation effect (PRE). The large magnitude of the paramagnetic effect provides sufficient sensitivity to allow for the observation of structures that are either transient or weakly populated, making it an excellent approach for studying the dynamic E2∼Ub species.

PRE Experiments Recapitulate the UbcH5c−Ub Noncovalent Complex. Our intention was to observe line broadening effects of spin-labeled Ub on an E2 to which it is conjugated. In light of the dynamic behavior described above, we first sought to ascertain whether broadening effects are detectable in a short-lived, transient species. We used a previously characterized low-affinity (noncovalent) complex formed between wild-type UbcH5c and Ub as a test case [PDB entry 2FUH (*15*)]. Ub-K48SL (1 molar equiv) was added to [^{15}N]UbcH5c, and HSQC-TROSY spectra were recorded in the absence ("active") and presence ("reduced") of ascorbate. Peak intensities were measured in both spectra, and the ratios of active to reduced intensities were used as indicators for residues in the proximity of the paramagnetic probe. A majority of UbcH5c resonances exhibit a ratio close to 1.0, indicating that these resonances are not affected by the spin-label and confirming that there are no nonspecific interactions between the spin-label and the E2. The strongest effect is observed for UbcH5 residue G27, as this resonance is undetectable in the active spectrum. Residues that were significantly affected by the spin-label were identified as those with ratios differing from the mean by more than one standard deviation. When mapped onto the three-dimensional structure, the affected residues define a surface that coincides with what is expected for the solution structure determined on the basis of observed NOEs (Figure 4A and Table S3 of the Supporting Information) (*15*).

Investigation of E2∼Ub Conformations: E2∼UbSL Experiments Indicate a Range of Conformations within the Conjugate. HSQC-TROSY spectra were recorded for the active and ascorbate-reduced [^{15}N]UbcH5c-O∼UbSL (with the S22R mutation) and [^{15}N]Ubc13-O∼UbSL conjugates for each spin-label position in Ub (residues 11, 39, 48, and 63). Spectra in which 1 molar equiv of each UbSL was added but not conjugated

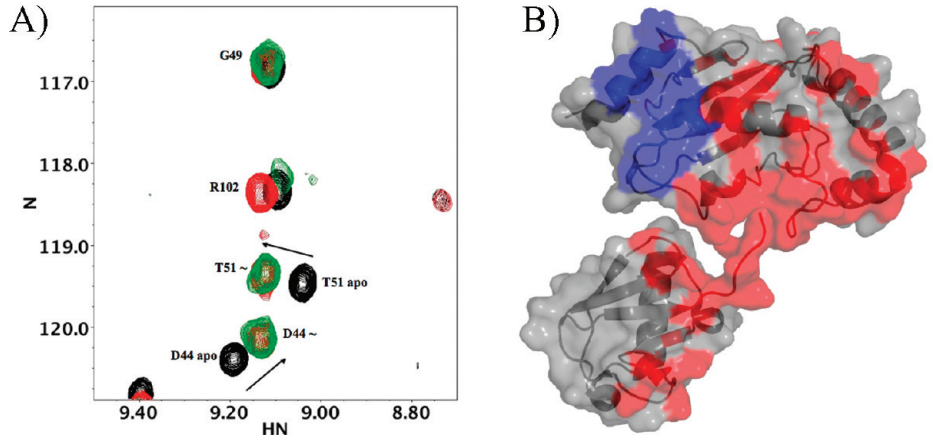

FIGURE 2: E3 binding does not disrupt the closed state. (A) 2D HSQC-TROSY spectrum of [^{15}N]Ubc13 (black) overlaid with those of the [^{15}N]Ubc13-O∼Ub conjugate (red) and the [^{15}N]Ubc13-O∼Ub conjugate with 1.1 molar equiv of BRCA1 1−112/BARD1 25−139 RING domains (green). Ubc13 residues D44 and T51, which are perturbed upon conjugation with Ub, are not affected by binding of BRCA1 to the E2∼Ub conjugate, indicating the Ubc13∼Ub conjugate can adopt the closed conformation even when bound to BRCA1. (B) CSPs of > 0.05 ppm upon addition of 1.1 equiv of RING E3 BRCA1/BARD1 mapped in blue on the structure of the Ubc13∼Ub conjugate [PDB entry 2GMI with the human Ubc13 structure overlaid (PDB entry 1J7D)]. CSPs upon conjugation to Ub as in Figure 1C are mapped in red.

to the [^{15}N]UbcH5c∼Ubc13 conjugate were also recorded as controls for potential intermolecular spin-label effects. In general, the E2 + Ub-SL spectra showed no peaks affected by the spin-label, with the exception of small effects observed on the "backside" of UbcH5c in the K48SL and K11SL cases, most likely a result of some residual noncovalent interaction with Ub despite the S22R mutation (see Experimental Procedures). These small backside effects were also observed in UbcH5c-O∼Ub experiments (Figure 5). Several lines of evidence confirm that the modification of Ub with TEMPO does not alter its structural or functional properties. First, Ub-K11SL functions like wild-type Ub in an in vitro ubiquitination assay with UbcH5c and BRCA1/BARD1 (Figure S1 of the Supporting Information). Second, spectral overlays of reduced PRE experiments at all spin-label positions show no significant differences in the E2 spectra (Figure S2 of the Supporting Information).

Results for the four spin-label positions in the UbcH5c-O∼Ub and Ubc13-O∼Ub conjugates are summarized in Table 1, and residue-level histograms of intensity ratios for each species are included in Figure S4 of the Supporting Information. In every spectral pair, the measured intensity ratio averaged over all E2 resonances is close to 1.0, confirming a lack of nonspecific intensity loss that might be expected to affect random surface residues to some extent. The average measured intensity ratio over all data sets is 0.98 for both E2s, indicating that the samples and spectra were well-matched and providing a high level of confidence in the intensities measured. Of the four Ub spin-label positions, K48 gives the strongest PRE in the context of the UbcH5c-O∼Ub conjugate, with a lowest intensity ratio of 0.2 for residues E122 and R131. In the context of the Ubc13-O∼Ub conjugate, the spin label at positions K11, D39, and K63 give strong effects. Ratios of 0.25 were observed for Ubc13 residues I108 for spin label position K11, and Ubc13 residues K82 and A122 for spin label position D39. Of particular note is the clear difference in the K63 position, which gives strong effects in the Ubc13-O∼Ub conjugate (lowest ratio being 0.1) but shows no significant effects in the context of the UbcH5c-O∼Ub conjugate. Given the concurrence among all the E2-O∼Ub PRE data sets, we chose to use a global threshold of 0.7 as the intensity ratio below which significance was assigned (i.e., an intensity loss that was > 30% of a peak's original intensity) (Table S3 of the Supporting Information).

Comparison of E2∼Ub Conjugates. Each of the four spin-label positions in the context of the UbcH5c-O∼Ub conjugate affects a unique set of resonances. Affected UbcH5 residues reside in the crossover helix, the active site and C-terminal helices, and loop 6. No single orientation of Ub relative to UbcH5 can satisfy all the observations, consistent with the flexible nature of the conjugate. To satisfy all the PRE effects, the conjugated Ub moiety must swing via its flexible C-terminal residues from closed conformations in which it approaches the E2 crossover helix, through extended conformations in which it resides below the active site and C-terminal helices, and up to loops 5 and 6 in "backbent" conformations (Figure 5, left). Considering the two sequential glycines at the C-terminus of Ub, remarkably little "twisting" of ubiquitin's C-terminal tail is required to move among these radically different conformations. Like the UbcH5c-O∼Ub conjugate, no single Ubc13-O∼Ub conformation can satisfy all of the PRE-affected surfaces. Together, the four spin-label positions suggest a Ub trajectory similar to that in the UbcH5c-O∼Ub conjugate, except that the Ub moiety must twist to allow its hydrophobic I44 surface to face the two sides of the E2, as indicated by the effect of K48SL observed on both the C-terminal helices and the β-sheet (Figure 5, right).

Small-Angle X-ray Scattering (SAXS) of the E2∼Ub Conjugates Confirms NMR-Based Models. SAXS curves for samples of UbcH5c, His$_6$-Ubc13, the UbcH5c-O∼Ub conjugate, and the His$_6$-Ubc13-O∼Ub conjugate were recorded at 25 °C (Figure 6A,B). No concentration-dependent effects or radiation damage was observed. Preliminary analysis of SAXS curves offers information about the shape (R_g) and size (D_{max}) of the sample proteins. The two free E2s give similar values for R_g and D_{max} that are consistent with monomeric E2s based on their known structures. UbcH5c-O∼Ub and His$_6$-Ubc13-O∼Ub conjugates also give similar values for R_g (23.0 and 23.7 Å, respectively) and D_{max} (70 and 75 Å, respectively). A D_{max} value of approximately 72 Å is predicted for the open conformation of the Ubc13-O∼Ub conjugate observed in the crystal structure (PDB entry 2GMI). Thus, the SAXS data indicate that extended conformations are populated in solution both by the Ubc13∼Ub conjugate and by the UbcH5c∼Ub conjugate.

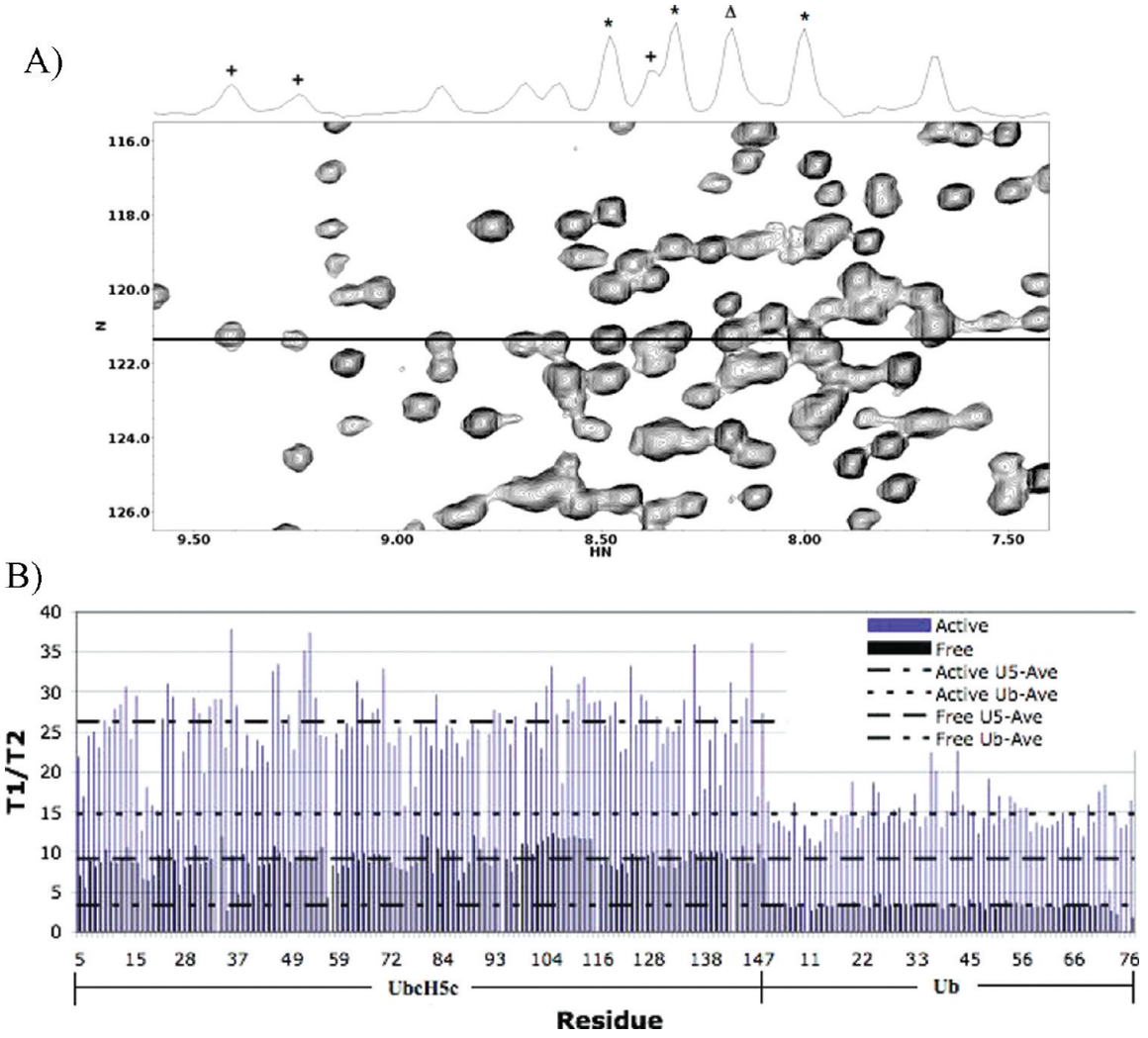

FIGURE 3: NMR resonance line widths and intensities indicate that the E2∼Ub conjugate is a dynamic species. (A) 2D HSQC-TROSY spectrum of the [^{15}N]Ubc13-O∼[^{15}N]Ub showing two classes of peaks based on intensity. In general, peaks that are sharper (more intense) arise from Ub residues, while the broader (weaker) peaks arise from Ubc13 residues. A one-dimensional slice taken at the ^{15}N frequency denoted by the black horizontal line in the 2D spectrum illustrates the distinction between Ub (*) and Ubc13 (+) resonances. A limited number of more intense Ubc13 resonances are observed (Δ); these arise from residues in loops or near the C-terminus. Off-center peaks are not labeled. (B) Histogram of T_1/T_2 values for UbcH5c and Ub residues in their conjugated (blue) and free (black) forms.

We reasoned the five atomic-level structures of E2∼Ub species (or their mimics) available in the PDB may represent a sampling of the allowable conformations available to E2∼Ub conjugates. Therefore, the structures were used as a basis set for further analysis of the SAXS data. Theoretical scattering curves were generated for each of the five E2∼Ub structures using CRYSOL and OLIGOMER for comparison with the measured curves for UbcH5c-O∼Ub and Ubc13-O∼Ub conjugates (Figure S5 of the Supporting Information). Not surprisingly, no single structure produced a theoretical scattering curve that fits the experimental data (Figure S6A of the Supporting Information). Furthermore, no linear combination of two, three, four, or five conformations chosen from a pool of existing E2∼Ub structures could recapitulate the experimental curves [OLIGOMER (Figure 6A,B)]. Among all possible combinations, conformations from the 2KJH and 1FXT structures fit the experimental data of the UbcH5c∼Ub conjugate with a χ^2 of 5.45, while conformations of the Ubc13∼Ub conjugate from the 3JW0 and 1FXT structures fit the data with a χ^2 of 3.87 (Figure S6B of the Supporting Information). Flexible systems such as the E2∼Ub conjugate, however, likely populate a continuum of conformations that may differ from existing determined structures.

To better account for the flexibility of the E2∼Ub conjugate, an ensemble optimization method (RanCh/GAJOE) was used to search for a minimal ensemble of UbcH5c∼Ub orientations that recapitulate the experimental data. Our initial analysis of the UbcH5c-O∼Ub conjugate was based upon a 20-member ensemble [generated from a pool of 10000 random conformations (see Experimental Procedures)] and included Ub orientations ranging from a closed state in which Ub is proximal to the E2 crossover helix, to an extended or open state in which Ub hangs below the E2 active site and C-terminal helices, to a backbent state in which Ub has swung to the opposite face of the E2 and is proximal to loops 5 and 6 [χ^2 value of 2.26 (Figure 6A)]. The ensemble shows a slight preference for extended E2∼Ub conformations, consistent with the weak CSPs observed in Ub upon conjugation to UbcH5c.

In contrast to the UbcH5∼Ub ensemble, a 20-member Ubc13∼Ub ensemble contains more conformers that represent a closed conformation with additional conformations that include the extended state and a weakly populated conformation placing Ub near the surface of Ubc13 that also binds Mms2 (χ^2 value of

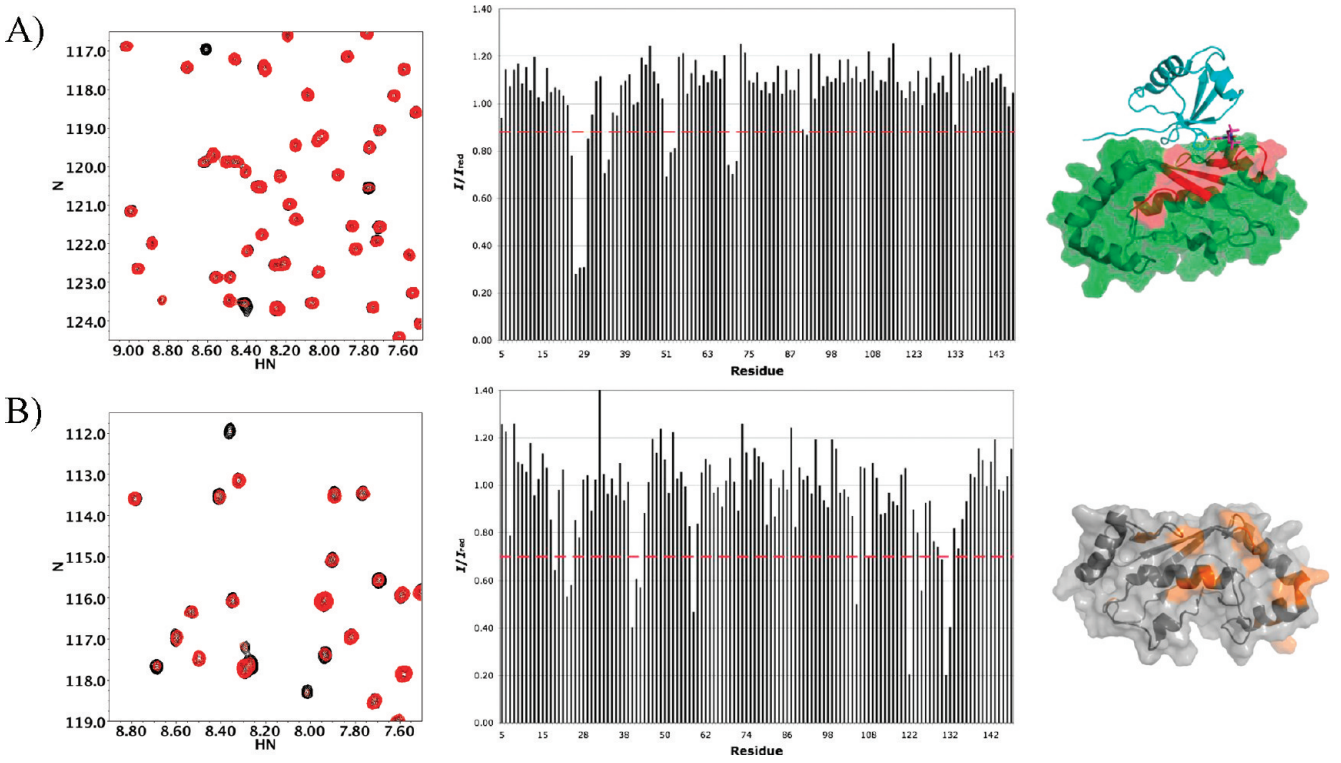

FIGURE 4: Paramagnetic relaxation enhancement data analysis. (A) 2D HSQC-TROSY spectra of [^{15}N]UbcH5c with 1 molar equiv of Ub-K48SL before (red) and after reduction with ascorbate (black, left). Peak intensities were measured and plotted as I/I_{red} ratios (center). Residues corresponding to intensity ratios of less than one standard deviation from the mean were mapped onto the 3D structure (right). (B) Same as panel A for the [^{15}N]UbcH5c-O∼Ub-K48SL conjugate.

2.75) (see Figure 6B). The highly populated closed state observed in the SAXS ensemble coincides with the CSPs observed upon formation of the Ubc13∼Ub conjugate.

In both cases, the ensembles of 20 E2∼Ub models represent one possible set of conformations that fit the data, and fine structural details should be analyzed in that light. Repeating the calculations to obtain additional ensembles, however, resulted in similar trends for both the pattern and density of E2∼Ub orientations, with associated χ^2 values remaining consistent in each case (Figure S6C of the Supporting Information). Furthermore, calculated ensembles comprised of fewer models yielded similar trends in E2∼Ub conformations and comparable χ^2 values (Figure S6D,E of the Supporting Information). Ensembles comprised of fewer than five structures were unable to satisfy both the pattern and density of E2∼Ub models observed in larger ensembles and, as a result, yielded poorer χ^2 values. Although there is little statistical difference between ensembles containing five or 20 models, we believe that a 20-member ensemble better reflects properties of an E2∼Ub species as it reveals sparsely populated conformations.

DISCUSSION

E2∼Ub species are essential components of the multiprotein complex required for the transfer of Ub to substrates. Several recent crystal structures and static NMR-based models have significantly increased the amount of structural information available, but the solution-state behavior of E2∼Ub conjugates reported here and previously by other groups (*22*, *23*) suggests that such structures provide a snapshot of what is a conformationally dynamic species. Here we present a more comprehensive description of the conjugate forms of two human E2s, UbcH5c and Ubc13, and find distinct differences between the two closely related E2s.

The NMR spectral features of both UbcH5c∼Ub and Ubc13∼Ub conjugates are consistent with flexibly linked domains, as indicated by line width analysis and ^{15}N relaxation data. Chemical shift perturbations, paramagnetic relaxation enhancement, and small-angle X-ray scattering identify distinct features of the two E2∼Ub species. Despite the strong CSPs observed in Ubc13 and Ub upon conjugation, analyses of line width, PRE, and SAXS data indicate a flexible species that inhabits multiple E2∼Ub conformations. Chemical shift perturbations suggest that the preferred state of the flexibly linked Ub is folded up toward the crossover helix of Ubc13, in what we call the closed conformer. Notably, the Ub swings "backward" toward loop 4 and β-strand 4 of Ubc13 more rarely than it swings up into the closed conformation, based upon SAXS and CSP data. This is in contrast to the behavior of the UbcH5c∼Ub conjugate, which appears to prefer a more open state, based on analysis of SAXS data and the general lack of Ub CSPs upon activation. Another notable difference is in Ub's C-terminus: PRE data indicate that the I44 hydrophobic face of Ub approaches both the front and back of Ubc13, implying that a twist in the Ub C-terminus must occur, whereas there is no evidence that the UbcH5c∼Ub conjugate undergoes such a pronounced twist.

Currently, there are two deposited crystal structures of the UbcH5∼Ub conjugate. In one structure (PDB entry 3A33), the conjugated Ub is in a conformation similar to the backbent orientation included in the UbcH5c∼Ub ensemble (*6*). The other is a structure of a complex formed between the UbcH5b∼Ub conjugate and the HECT-type E3, Nedd4L (*7*). In this case, the conjugated Ub is in an extended−twisted

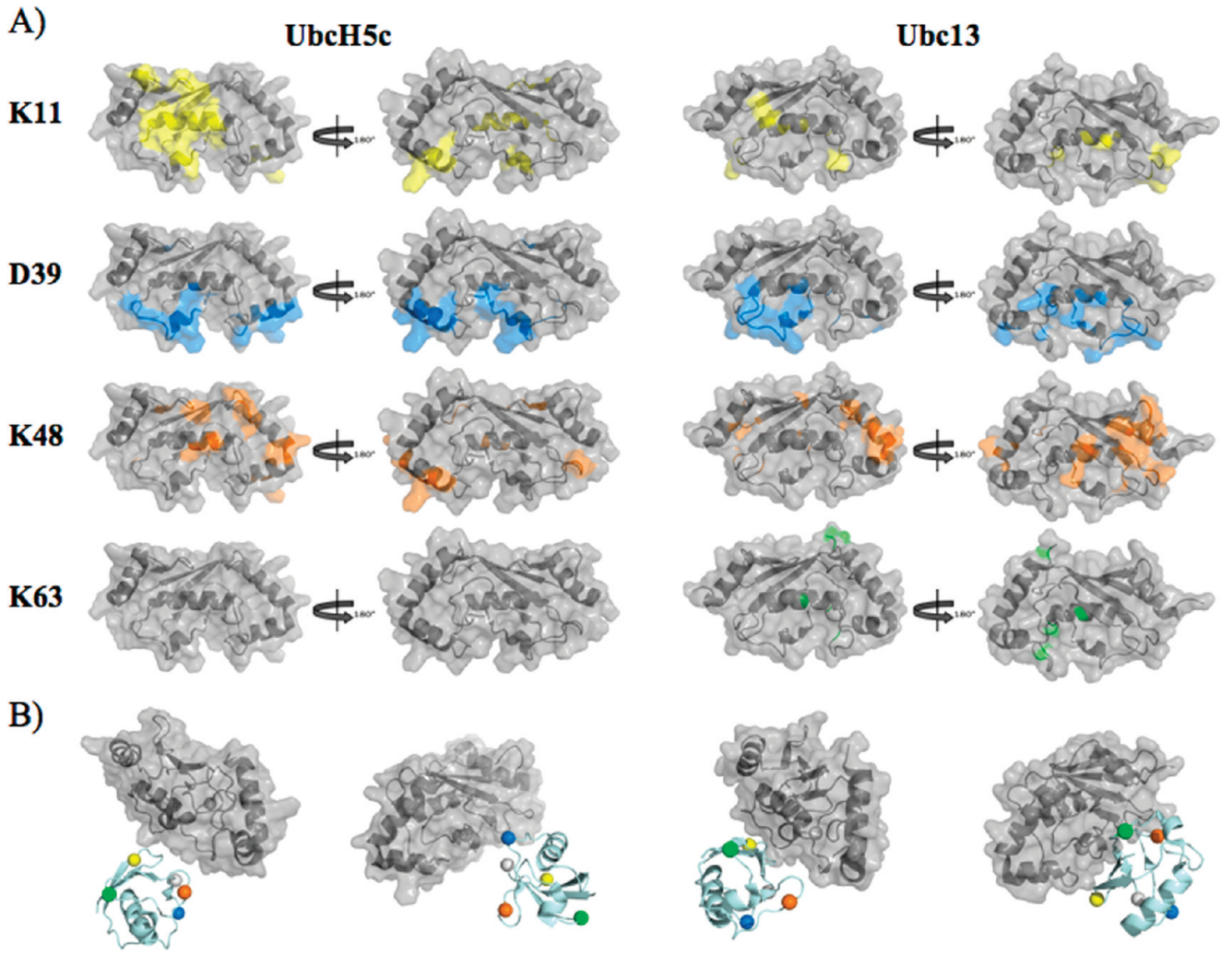

FIGURE 5: Observed PREs are specific to both spin-label position and E2 identity. (A) Highlighted residues in UbcH5c (PDB entry 2FUH, left) and Ubc13 (PDB entry 1J7D, right) are those whose resonances show PRE effects upon conjugation with Ub-SL at positions K11 (yellow), D39 (blue), K48 (orange), and K63 (green). Colored residues correspond to HSQC peaks with an I/I_{red} intensity ratio of ≤0.7. (B) Illustrative extreme E2∼Ub conformations. SL positions shown as colored spheres to match affected regions shown above; the Ub core C-terminus and E2 active sites are shown as gray spheres.

Table 1: Comparison of the Spin-Label Effects for UbcH5c-O−Ub and Ubc13-O−Ub Conjugates and UbcH5c with Ub

	average I/I_{red} ratio	standard deviation	lowest I/I_{red} ratio	residue with the lowest I/I_{red} ratio	no. of significant residues
UbcH5c-O∼Ub					
K11SL	0.9	0.22	0.36	109	21
D39SL	0.9	0.22	0.38	84 and 87	23
K48SL	0.96	0.22	0.2	122 and 131	14
K63SL	1.14	0.12	0.86	94	0
Ubc13-O∼Ub					
K11SL	0.93	0.16	0.25	108	8
D39SL	0.88	0.22	0.25	82 and 122	18
K48SL	0.96	0.21	0.38	134	17
K63SL	1.13	0.2	0.1	149	4
UbcH5c with Ub					
K48SL	1.06	0.2	0.28	26	14

conformation that places Ub residue D39 near UbcH5 loop 8, a state that is also included in the UbcH5c∼Ub ensemble. These structures suggest how additional binding interactions may select a particular E2∼Ub conformation from among manifold possibilities.

The conjugation-induced CSPs in human Ubc13 agree with a previous report (*24*), although our complete $^{15}N-^{1}H$ assignments afford a more detailed view of the Ubc13∼Ub species. An extended state of the Ubc13∼Ub conjugate as observed in the crystal structure (PDB entry 2GMI) is represented among the conformations in the solution ensemble. The presence of the Ubc13 binding partner, Mms2, which can interact with a Ub moiety from another Ubc13∼Ub conjugate, may shift the equilibrium toward the extended state seen in the crystal. It is

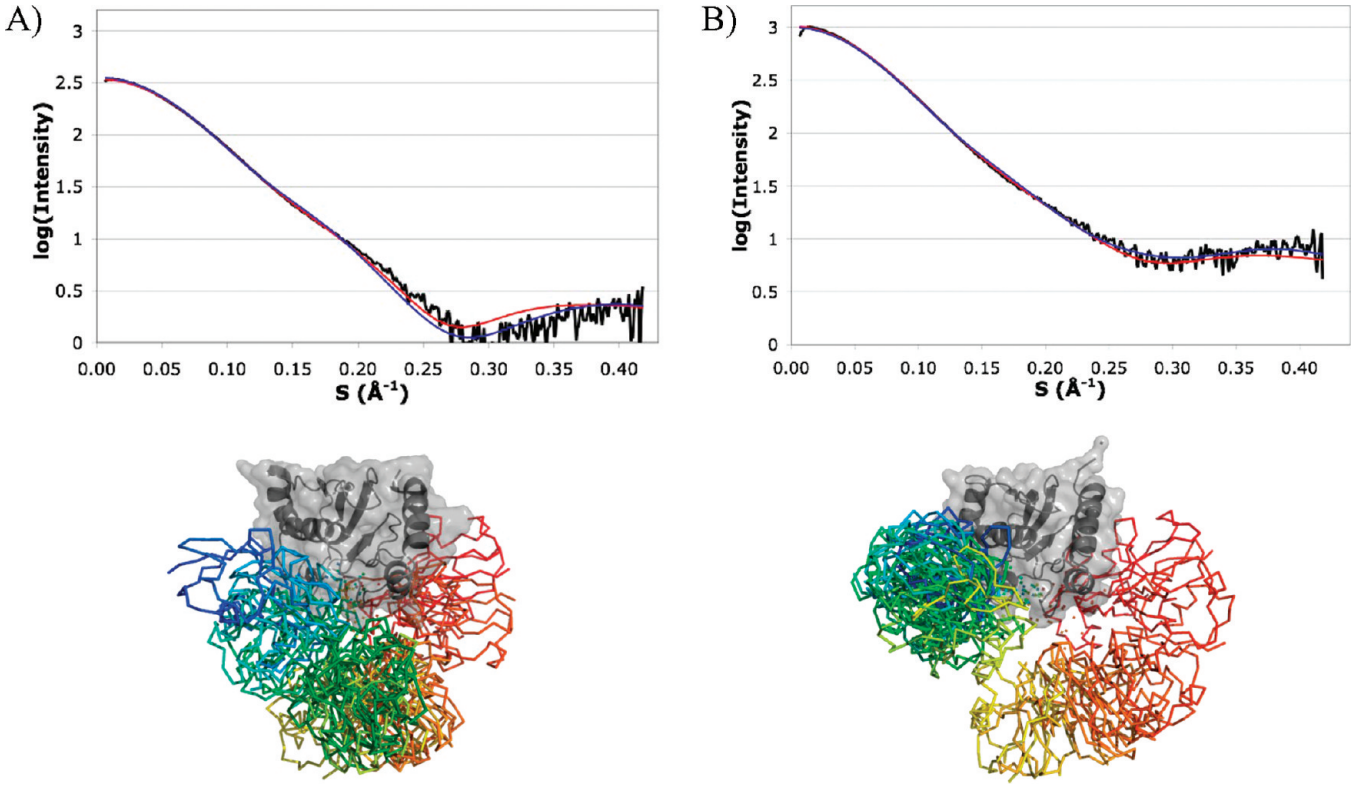

FIGURE 6: Analysis of SAXS curves reveals a range of E2∼Ub conformations. (A) Experimental SAXS data of the UbcH5c-O∼Ub conjugate (top, black) overlaid with calculated fits produced from OLIGOMER (blue, based on five published E2∼Ub structures) and EOM (red, RanCh/GAJOE) analysis. An ensemble of 20 UbcH5c∼Ub conformations produced by EOM analysis is also shown (bottom). (B) Same as panel A for the Ubc13-O∼Ub conjugate.

beyond the technical scope of this study to characterize the conjugated Ubc13−Mms2 heterodimer in solution, so we cannot comment further on the effects of Mms2 binding. Overall, our results indicate that the Ubc13∼Ub conjugate populates a closed state with the highest frequency. Furthermore, our NMR data indicate that binding of the RING E3 BRCA1/BARD1 to the Ubc13∼Ub conjugate does not preclude the closed state observed in the ensemble.

There are a growing number of reports of proteins that selectively recognize E2∼Ub conjugates, but not the free protein components. To date, three proteins have been identified that specifically bind an E2∼Ub conjugate: bacterial E3 ligase SspH2 (binds the UbcH5c∼Ub conjugate) (*23*), bacterial effector protein OspG (binds the UbcH5b∼Ub conjugate) (*25*), and nuclear import protein importin-11 (binds the UbcM2∼Ub conjugate) (*26*). Ub and E2 enzymes individually contain a number of potential binding sites; conjugation of the two proteins creates new combinatorial possibilities that may create unique binding modes. On the basis of the two crystal structures available, it appears that (at least in these cases) interacting proteins make use of available E2∼Ub orientations in their modes of binding. Multiple conformations assumed by the E2∼Ub conjugate allow for diverse binding modes. Such flexibility allows the E2∼Ub conjugate to participate in a variety of complexes, ultimately resulting in diverse biological roles. Commonalities among E2∼Ub structures might be related to common binding partners. For example, neither the Ubc13∼Ub model nor the UbcH5c∼Ub model places Ub in an orientation that is likely to interfere with binding to a RING E3. On the other hand, differences in E2∼Ub structures could be linked to differences in binding partners, including noncanonical E3 ligases. As a result, studying molecular interactions with the free E2 may not directly translate to the E2∼Ub conjugate.

Despite the technical challenges posed, it is clear that studying the active, conjugated form of E2 Ub-conjugating enzymes can provide insights not readily apparent from the structures of isolated E2s. Understanding the combinatorial effect of E2 and Ub binding sites and the E2-specific conformational ensembles will be key to deciphering the E2 protein interactome. The NMR-based spin labeling approach described here will be generally applicable to the study of other E2∼Ub conjugates as well as to the study of E2∼Ub species in complex with interacting proteins, including E3 ligases.

ACKNOWLEDGMENT

We thank the Stanford Synchrotron Radiation Laboratory (SSRL) and the Pacific Northwest National Laboratory (PNNL) for beam time and the use of NMR spectrometers. Portions of this research were conducted at SSRL beamline 4-2, a national user facility operated by Stanford University on behalf of the U.S. Department of Energy, Office of Basic Energy Sciences. The SSRL Structural Molecular Biology Program is supported by the Department of Energy, Office of Biological and Environmental Research, and by the National Institutes of Health, National Center for Research Resources, Biomedical Technology Program. A portion of the research was performed using EMSL, a national scientific user facility sponsored by the Department of Energy's Office of Biological and Environmental Research and located at PNNL. We gratefully acknowledge Walter Chazin and members of the Klevit lab for helpful discussions and critical reading of the manuscript.

SUPPORTING INFORMATION AVAILABLE

Specific protein residues affected by PRE and CSP, as well as SAXS statistics, and E2 sequence alignments. This material is available free of charge via the Internet at http://pubs.acs.org.

REFERENCES

1. Pickart, C. M. (2001) Mechanisms underlying ubiquitination. *Annu. Rev. Biochem. 70*, 503–533.
2. Ye, Y., and Rape, M. (2009) Building ubiquitin chains: E2 enzymes at work. *Nat. Rev. Mol. Cell Biol. 10*, 755–764.
3. Eddins, M. J., Carlile, C. M., Gomez, K. M., Pickart, C. M., and Wolberger, C. (2006) Mms2-Ubc13 covalently bound to ubiquitin reveals the structural basis of linkage-specific polyubiquitin chain formation. *Nat. Struct. Mol. Biol. 13*, 915–920.
4. Hamilton, K. S., Ellison, M. J., Barber, K. R., Williams, R. S., Huzil, J. T., McKenna, S., Ptak, C., Glover, M., and Shaw, G. S. (2001) Structure of a conjugating enzyme-ubiquitin thiolester intermediate reveals a novel role for the ubiquitin tail. *Structure 9*, 897–904.
5. Serniwka, S. A., and Shaw, G. S. (2009) The structure of the UbcH8-ubiquitin complex shows a unique ubiquitin interaction site. *Biochemistry 48*, 12169–12179.
6. Sakata, E., Satoh, T., Yamamoto, S., Yamaguchi, Y., Yagi-Utsumi, M., Kurimoto, E., Tanaka, K., Wakatsuki, S., and Kato, K. (2010) Crystal structure of UbcH5b−ubiquitin intermediate: Insight into the formation of the self-assembled E2−Ub conjugates. *Structure 18*, 138–147.
7. Kamadurai, H. B., Souphron, J., Scott, D. C., Duda, D. M., Miller, D. J., Stringer, D., Piper, R. C., and Schulman, B. A. (2009) Insights into ubiquitin transfer cascades from a structure of a UbcH5B−ubiquitin-HECT(NEDD4L) complex. *Mol. Cell 36*, 1095–1102.
8. Ozkan, E., Yu, H., and Deisenhofer, J. (2005) Mechanistic insight into the allosteric activation of a ubiquitin-conjugating enzyme by RING-type ubiquitin ligases. *Proc. Natl. Acad. Sci. U.S.A. 102*, 18890–18895.
9. Huang, A., de Jong, R. N., Wienk, H., Winkler, G. S., Timmers, H. T. M., and Boelens, R. (2009) E2-c-Cbl recognition is necessary but not sufficient for ubiquitination activity. *J. Mol. Biol. 385*, 507–519.
10. Siepmann, T. J., Bohnsack, R. N., Tokgöz, Z., Baboshina, O. V., and Haas, A. L. (2003) Protein interactions within the N-end rule ubiquitin ligation pathway. *J. Biol. Chem. 278*, 9448–9457.
11. Haas, A. L., and Rose, I. A. (1982) The mechanism of ubiquitin activating enzyme. A kinetic and equilibrium analysis. *J. Biol. Chem. 257*, 10329–10337.
12. Michelle, C., Vourc'h, P., Mignon, L., and Andres, C. R. (2009) What was the set of ubiquitin and ubiquitin-like conjugating enzymes in the eukaryote common ancestor? *J. Mol. Evol. 68*, 616–628.
13. Moraes, T. F., Edwards, R. A., McKenna, S., Pastushok, L., Xiao, W., Glover, J. N. M., and Ellison, M. J. (2001) Crystal structure of the human ubiquitin conjugating enzyme complex, hMms2-hUbc13. *Nat. Struct. Mol. Biol. 8*, 669–673.
14. Brzovic, P. S., Keeffe, J. R., Nishikawa, H., Miyamoto, K., Fox, D., III, Fukuda, M., Ohta, T., and Klevit, R. (2003) Binding and recognition in the assembly of an active BRCA1/BARD1 ubiquitin-ligase complex. *Proc. Natl. Acad. Sci. U.S.A. 100*, 5646–5651.
15. Brzovic, P. S., Lissounov, A., Christensen, D. E., Hoyt, D. W., and Klevit, R. E. (2006) A UbcH5/ubiquitin noncovalent complex is required for processive BRCA1-directed ubiquitination. *Mol. Cell 21*, 873–880.
16. Delaglio, F., Grzesiek, S., Vuister, G. W., Zhu, G., Pfeifer, J., and Bax, A. (1995) NMRPipe: A multidimensional spectral processing system based on UNIX pipes. *J. Biomol. NMR 6*, 277–293.
17. Johnson, B. A., and Blevins, R. A. (1994) NMR View: A computer program for the visualization and analysis of NMR data. *J. Biomol. NMR 4*, 603–614.
18. Konarev, P. V., Volkov, V. V., Sokolova, A. V., Koch, M. H. J., and Svergun, D. I. (2003) PRIMUS: A Windows PC-based system for small-angle scattering data analysis. *J. Appl. Crystallogr. 36*, 1277–1282.
19. Svergun, D. I. (1992) Determination of the regularization parameter in indirect-transform methods using perceptual criteria. *J. Appl. Crystallogr. 25*, 495–503.
20. Svergun, D., Barberato, C., and Koch, M. H. J. (1995) CRYSOL: A Program to Evaluate X-ray Solution Scattering of Biological Macromolecules from Atomic Coordinates. *J. Appl. Crystallogr. 28*, 768–773.
21. Bernadó, P., Mylonas, E., Petoukhov, M. V., Blackledge, M., and Svergun, D. I. (2007) Structural Characterization of Flexible Proteins Using Small-Angle X-ray Scattering. *J. Am. Chem. Soc. 129*, 5656–5664.
22. Miura, T., Klaus, W., Gsell, B., Miyamoto, C., and Senn, H. (1999) Characterization of the binding interface between ubiquitin and class I human ubiquitin-conjugating enzyme 2b by multidimensional heteronuclear NMR spectroscopy in solution. *J. Mol. Biol. 290*, 213–228.
23. Levin, I., Eakin, C., Blanc, M.-P., Klevit, R. E., Miller, S. I., and Brzovic, P. S. (2010) Identification of an unconventional E3 binding surface on the UbcH5∼Ub conjugate recognized by a pathogenic bacterial E3 ligase. *Proc. Natl. Acad. Sci. U.S.A. 107*, 2848–2853.
24. McKenna, S., Moraes, T., Pastushok, L., Ptak, C., Xiao, W., Spyracopoulos, L., and Ellison, M. J. (2003) An NMR-based model of the ubiquitin-bound human ubiquitin conjugation complex Mms2. Ubc13. The structural basis for lysine 63 chain catalysis. *J. Biol. Chem. 278*, 13151–13158.
25. Kim, D. W., Lenzen, G., Page, A.-L., Legrain, P., Sansonetti, P. J., and Parsot, C. (2005) The *Shigella flexneri* effector OspG interferes with innate immune responses by targeting ubiquitin-conjugating enzymes. *Proc. Natl. Acad. Sci. U.S.A. 102*, 14046–14051.
26. Plafker, S. M., Plafker, K. S., Weissman, A. M., and Macara, I. G. (2004) Ubiquitin charging of human class III ubiquitin-conjugating enzymes triggers their nuclear import. *J. Cell Biol. 167*, 649–659.